Technical Note

Coupling Light Intensity and Hyperspectral Reflectance Improve Estimations of the Actual Electron Transport Rate of Mango Leaves (*Mangifera indica* L.)

Jia Jin [1] , **Quan Wang** [2,*] **and Jie Zhuang** [3]

1. Key Laboratory of Environment Change and Resources Use in Beibu Gulf, Ministry of Education, Nanning Normal University, Nanning 530001, China; jinjia@nnnu.edu.cn
2. Faculty of Agriculture, Shizuoka University, Shizuoka 422-8529, Japan
3. Graduate School of Science and Technology, Shizuoka University, Shizuoka 422-8529, Japan; zhuang.jie.21@shizuoka.ac.jp
* Correspondence: wang.quan@shizuoka.ac.jp; Tel.: +81-54-2383683

Abstract: Real-time and accurate assessment of the photosynthetic rate is of great importance for monitoring the contribution of leaves to the global carbon cycle. The electron transport rate is a critical parameter for accurate simulation of the net photosynthetic rate, which is highly sensitive to both light conditions and the biochemical state of the leaf. Although various approaches, including hyperspectral remote sensing techniques, have been proposed so far, the actual electron transport rate is rarely quantified in real time other than being derived from the maximum electron transport (J_{max}) at a reference temperature in most gas exchange models, leading to the decoupling of gas exchange characteristics from environmental drivers. This study explores the potential of using incident light intensity, hyperspectral reflectance data, and their combination for real-time quantification of the actual electron transport rate (J_a) in mango leaves. The results show that the variations in J_a could be accurately estimated using a combination of incident light intensity and leaf reflectance at 715 nm, with a ratio of performance to deviation (*RPD*) value of 2.12 (very good predictive performance). Furthermore, the J_a of sunlit leaves can be predicted with an *RPD* value of about 2.60 using light intensity and a single-band reflectance value within 760–1320 nm, while the actual electron transport rate of shaded leaves can only be predicted with a lower *RPD* value of 1.73 (fair performance) using light intensity and reflectance at 685 nm. These results offer valuable insights into developing non-destructive, rapid methods for real-time estimation of actual electron transport rates using hyperspectral remote sensing data and incident light conditions.

Keywords: electron transport rate; hyperspectral; light intensity; reflectance

1. Introduction

Photosynthesis in plants is a crucial process within terrestrial ecosystems, regulating carbon fluxes between ecosystems and the atmosphere [1]. Accurate measurement or estimation of photosynthesis is critical for monitoring the carbon cycle from individual leaves to the global scale [2]. Despite the critical importance of photosynthesis for terrestrial ecosystems, the global mapping of photosynthesis remains a challenge due to limited measurements at different scales and its complex interactions with environmental factors [3,4]. Among the various tools, the Farquhar–von Caemmerer–Berry (FvCB) model is a widely used biochemical model that describes the net CO_2 assimilation rate (An) in C3 plants [5,6] and provides a global view of photosynthetic properties. The model integrates several key physiological processes, with the electron transport rate (*J*) being a critical parameter for accurately simulating photosynthetic responses to environmental conditions [7]. Accurate modeling of the real-time electron transport rate allows for accurate simulation of photosynthetic responses to these environmental variables, which is critical for predicting plant behavior under different climatic conditions.

The electron transport rate is sensitive to both light conditions and the biochemical state of the leaf. In most leaf and canopy gas exchange models, the electron transport rate (J) is determined by the incident light intensity, the leaf's absorbance or light capture efficiency, the maximum electron transport rate (J_{max}), and the curvature factor that determines the transition of photosynthesis phases between different light conditions [8]. Among these input parameters, leaf absorbance and the curvature factor are usually assumed to have constant values [9]. However, leaf biochemical parameters, such as chlorophyll content and internal leaf structure, influence the light absorption capacity and thus the rate of electron transport in leaves [10,11]. A higher chlorophyll content generally leads to a higher electron transport rate because more light energy is captured for electron transport [12]. Therefore, radiation absorption in the PAR region is heavily influenced by the biochemistry and structural traits of plants [13]. On the other hand, the electron transport rate increases with light intensity up to a certain point [14]. The light response curve is a measure of the electron transport rate in a given system in response to light. It shows a rapid increase at low-to-moderate light levels, followed by a plateau at higher intensities [15–17]. Furthermore, the determination of J_{max} at a given temperature involves a temperature correction function and the ratio of J_{max} to the maximum rate of Rubisco activity (V_{cmax}) at 25 °C [18]. However, the ratio of J_{max}:V_{cmax} is highly variable due to species, season, and leaf position in the plant canopy [19,20]. Since all aforementioned facts may introduce errors into the calculation of the actual electron transport rate [18], real-time estimation of it remains a challenge.

Alternatively, solar-induced fluorescence (SIF) is closely connected to the photosynthetic electron transport chain, as both processes involve the absorption of light and the subsequent excitation of chlorophyll molecules [21]. Thus, it has been proposed that the actual electron transport rate (J_a) can be determined from chlorophyll fluorescence parameters [9,22]. However, the relationship between SIF and photosynthetic activity has been shown to vary among different plant types, growth stages, sky conditions, and time scales [23–28]. Furthermore, accurate detection of solar-induced chlorophyll fluorescence in plants is inherently challenging because only a small fraction of absorbed photons (typically $\leq 5\%$) is re-emitted as fluorescence [29–31]. Although SIF provides a means to monitor the electron transport rate, using SIF to estimate the electron transport rate requires sophisticated instrumentation and data processing techniques [9].

Hyperspectral reflectance has become a valuable tool for estimating the biochemical status of leaves [32,33]. By capturing detailed spectral information across a broad range of wavelengths, hyperspectral imaging enables precise detection and quantification of various biochemical constituents in plant leaves [34]. This technique enables a non-destructive, rapid, and detailed assessment of a plant's biochemical parameters, which is essential for plant physiological research. Recently, many statistical regression techniques have been proposed and applied to retrieve photosynthetic capacity parameters from hyperspectral reflectance spectra. Spectral vegetation indices and multiple regressions have been applied to estimate V_{cmax} and J_{max} from hyperspectral reflectance [35–39]. However, most of them focus on V_{cmax} and J_{max} at a reference [35,37,38,40] rather than the actual real-time electron transport rate.

This study was inspired by Liran et al. (2020), who proposed a model for electron transport rates based on a combination of solar-induced fluorescence, the NDVI (normalized difference vegetation index), and light intensity [41]. This model has been validated on crops such as lettuce (*L. sativa*) and maize (*Z. mays*), showing a strong correlation with traditional fluorometer measurements [41]. The estimation of photosynthesis from fluorescence is based on the electron transport rate, which can be calculated as PAR × leaf absorbance × fluorescence-related parameters [9,21,42]. Given that fluorescence parameters can be effectively monitored by combining hyperspectral reflectance with light drivers [43,44], the combination of light drivers and reflectance to directly track the electron transport rate is worth exploring.

Therefore, this study addresses the potential application of combining incident light intensity and hyperspectral reflectance data for real-time quantification of the actual leaf electron transport rate. Thus, the main objectives of this study focus on (1) exploring the variations in the actual electron transport rate under different incident light levels and the feasibility of estimating *J* directly from light conditions; (2) investigating the potential of using leaf reflectance-based vegetation indices to estimate the actual electron transport rate; (3) determining the feasibility of estimating the actual electron transport rate based on a combination of incident light intensity and leaf reflectance information.

2. Materials and Methods

2.1. Measurements of Leaf Gas Exchange for the Determination of the Actual Electron Transport Rate and Leaf Reflectance

Leaf gas exchange and reflectance measurements were conducted to determine the actual electron transport rate in mango leaves *(M. indica* L.) at the Baise National Agricultural Sci-tech Zone in Guangxi, China. Sampling took place from 7 August to 1 September 2021, using the detached branch method at an Integrated Remote Sensing Experimental Site for mango trees (23°42′09.5″N, 106°59′42.2″E) [45]. Fully expanded mature leaves at the top and bottom of the canopy were classified as sunlit and shaded, respectively. Branches with at least four leaves were collected daily before sunrise from 7 August to 1 September 2021, using the detached branch method. A total of 590 measurements were collected and used for the analysis.

The gas exchange data for the mango leaves were recorded with the use of an LI-6800 portable photosynthesis system (LI-COR Inc., Lincoln, NE, USA) [46]. The CO_2 concentration entering the cuvette and the automatic flow control were set to 400 μmol CO_2 mol^{-1} and 500 μmol s^{-1}, respectively. The chamber temperature was set to ambient, and the humidity was set to 55%. Measurements were made at ten different light intensities. The PAR (photosynthetically active radiation) values ranged from 200 to 2000 μmol m^{-2} s^{-1}, including 200, 400, 600, 800, 1000, 1200, 1400, 1600, 1800, and 2000 μmol m^{-2} s^{-1}. Initially, the light source was 90% red and 10% blue. Blue light levels were progressively raised, and red light levels were reduced in 10% increments. The leaves were allowed to acclimate to a specific light intensity and quality for a minimum of 20 min, and gas exchange parameters were recorded as soon as ΔH_2O and ΔCO_2 had stabilized. Immediately after each gas exchange measurement, leaf reflectance (from 350 to 2500 nm) was recorded by using an ASD field spectroradiometer (Analytical Spectral Devices Inc., Boulder, CO, USA) attached to a leaf clip. Further details of the synchronous measurement procedure can be found in [46,47]. The measured reflectance spectra of sunlit and shaded leaves are shown in Figure 1.
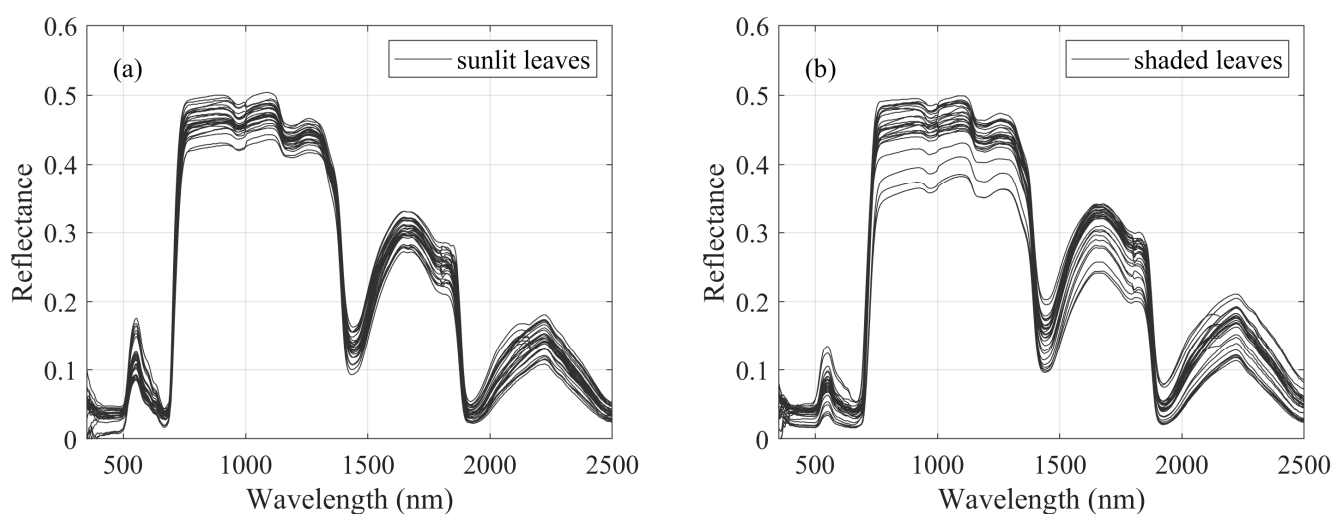

Figure 1. Variations in spectra of sunlit (**a**) and shaded (**b**) leaves.

The FvCB biochemical model has been widely used in many land surface models to compute photosynthesis for C3 species [6,48]. The actual electron transport rate (J_a) can be calculated based on the net photosynthesis (A_n) and respiration (R_d) [9,18]:

$$J_a = A_g \cdot \frac{4C_i + 8\Gamma^*}{C_i - \Gamma^*} = (A_n + R_d) \cdot \frac{4C_i + 8\Gamma^*}{C_i - \Gamma^*} \tag{1}$$

A_g represents the gross photosynthesis; R_d is the day respiration; C_i is the intercellular CO_2 concentration; Γ^* represents the CO_2 compensation point in the absence of mitochondrial respiration in the light for C3 plants; and J_a stands in for the actual electron transport rate balanced by carboxylation and photorespiration in the carbon reactions.

The CO_2 compensation point in the absence of mitochondrial respiration (Γ^*) can be calculated from the air temperature [49]:

$$\Gamma^* = 36.9 + 1.18(T - 25) + 0.036(T - 25)^2 \tag{2}$$

2.2. Hyperspectral Reflectance and Vegetation Indices for Tracing the Actual Electron Transport Rate

There are various hyperspectral vegetation indices and most of them can be categorized into several general types [50]. Most published indices can be expressed as single-band reflectance (R), two-band reflectance difference (D), the two-band simple ratio (SR), and two-band normalized difference (ND) [51]. In this study, these four commonly used spectral index types were investigated to trace the variation in J_a.

All possible combinations of bands within the 350–2500 nm range (listed in Table 1) for the *VI* (vegetation index) were tested for J_a estimation using polynomial regression (linear to the first order) or logarithmic regression methods.

$$J_a = \beta_1 \cdot VI + \beta_0 + \varepsilon \tag{3}$$

$$J_a = \beta_1 \cdot \ln(VI) + \beta_0 + \varepsilon \tag{4}$$

where β represents the fitting coefficient; and ε is the modeling error.

Table 1. The index types and spectral band combinations used for this study.

	Index Type	Index Formula	Band Combinations
1.	R($\lambda1$)	$= R_{\lambda1}$	$\lambda1 \in [350, 2500]$
2.	SR($\lambda1, \lambda2$)	$= \frac{R_{\lambda1}}{R_{\lambda2}}$	$\lambda1 \in [350, 2500], \lambda2 \in [350, 2500], \lambda1 \neq \lambda2$
3.	D($\lambda1, \lambda2$)	$= R_{\lambda1} - R_{\lambda2}$	$\lambda1 \in [350, 2500], \lambda2 \in [350, 2500], \lambda1 \neq \lambda2$
4.	ND($\lambda1, \lambda2$)	$= \frac{(R_{\lambda1} - R_{\lambda2})}{(R_{\lambda1} + R_{\lambda2})}$	$\lambda1 \in [350, 2500], \lambda2 \in [350, 2500], \lambda1 \neq \lambda2$

A correlation analysis was conducted on each *VI* and the actual electron transport rate to investigate their relationship. In order to enhance computational efficiency, the five-point center average method was used, and the reflectance data were resampled to 5 nm.

2.3. Composite Model Development and Statistical Criteria

To explore the ability of leaf reflectance to describe J_a under different PAR conditions, parsimonious models were constructed to estimate J_a using polynomial regression (first-order linear) and logarithmic regression methods. J_a was first estimated using both PAR and vegetation indices (*VIs*) derived from leaf reflectance.

The J_a models were obtained as follows:

$$J_a = \beta_1 \cdot PAR \cdot VI + \beta_0 + \varepsilon \tag{5}$$

$$J_a = \beta_1 \cdot \ln(PAR \cdot VI) + \beta_0 + \varepsilon \tag{6}$$

where β represents the fitting coefficient; and ε is the modeling error.

The coefficient of determination (R^2), the root mean square error by mean (*RMSE*), the ratio of performance to deviation (*RPD*), and the corrected Akaike information criterion (*AICc*) [52] were calculated and used as the statistical criteria to evaluate the models:

$$R^2 = 1 - \frac{\sum_i^n (Y_i - \hat{Y}_i)^2}{\sum_i^n (Y_i - \overline{Y})^2} \tag{7}$$

$$RMSE = \sqrt{\frac{1}{n}\sum_i^n (Y_i - \hat{Y}_i)^2} \tag{8}$$

$$RPD = \frac{Sd}{SEP} \tag{9}$$

$$AICc = \ln\left(\frac{RSS}{n}\right) + \frac{n+m}{n-m-2} \tag{10}$$

where Y is the measured J_a value, $\hat{Y}$ is the model-estimated J_a value, $\overline{Y}$ is the average value of J_a for all samples, n is the leaf sample number, Sd is the standard deviation of J_a, SEP is the standard error of prediction (calculated as the root mean squared error here), m is the number of model parameters, and RSS refers to the residual sum of squares.

According to the *RPD* values, the models can be classified into the following groups: excellent (models with $RPD \geq 2.5$), very good (models with $2.0 \leq RPD < 2.5$), good (models with $1.8 \leq RPD < 2.0$), fair (models with $1.4 \leq RPD < 1.8$), poor (models with $1.0 \leq RPD < 1.4$), and very poor (models with $RPD < 1.0$) [53].

3. Results

3.1. Variations in Actual Electron Transport Rate under Different Light Intensities

The impact of light intensity (PAR, $\mu mol\ m^{-2}\ s^{-1}$) on the electron transport rate was examined, and the correlation between PAR and J_a was plotted in Figure 2a. In general, the shaded leaves had lower actual electron transport rates than the sunlit leaves. The scatter plot suggests a significant correlation between the actual electron transport rate and incident light intensity, as indicated by the R^2 value. The actual electron transport rate of mango leaves increased with light intensity. The polynomial regression method (first-order linear) involving the incident light intensity could follow the variation in J_a, with an R^2 of 0.68, an *RPD* of 1.76, and an *RMSE* of 11.60 $\mu mol\ m^{-2}\ s^{-1}$ (Figure 2a). The logarithmic regression model was more effective in capturing the variation in J_a, with an R^2 of 0.73, an *RPD* of 1.92, and an *RMSE* of 10.65 $\mu mol\ m^{-2}\ s^{-1}$ (Figure 2c).
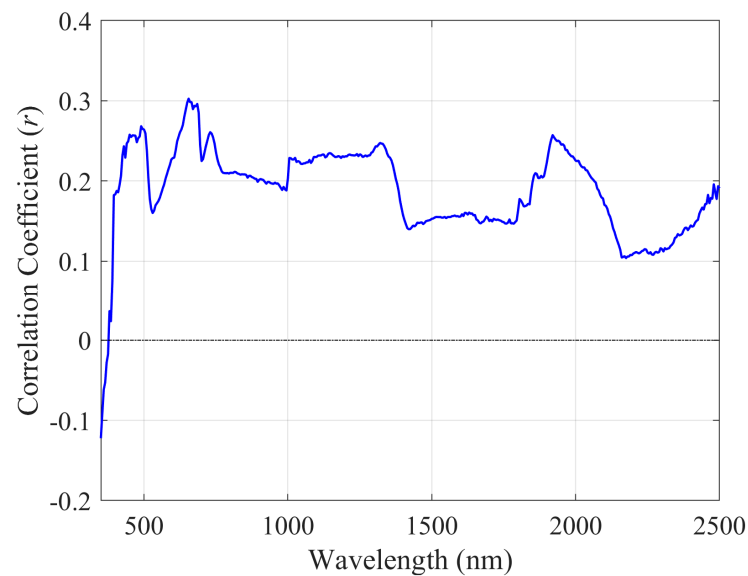
However, the actual electron transport rate of different leaves varied significantly under the same incident light intensity level. Therefore, the characteristics of different leaves should be considered when estimating the electron transport rate. The logarithmic regression model was excellent for capturing the variation in J_a in sunlit leaves, with an R^2 of 0.90, an *RPD* of 3.21, and an *RMSE* of 6.62 $\mu mol\ m^{-2}\ s^{-1}$ (Figure 2c). Meanwhile, the logarithmic regression model was good at describing the variation in J_a in shaded leaves, with an R^2 of 0.69, an *RPD* of 1.80, and an *RMSE* of 10.05 $\mu mol\ m^{-2}\ s^{-1}$ (Figure 2d).

3.2. Relationship of Actual Electron Transport Rate with Hyperspectral Reflectance and Vegetation Indices

The correlation coefficients (r) between the actual electron transport rate and leaf reflectance at each wavelength are displayed in Figure 3. It was found that leaf reflectance values from 400 to 2500 nm were positively correlated with the actual electron transport rates. Leaf reflectance values around 490 nm, 655 nm, 730 nm, and 1920 nm were significantly correlated with J_a (r > 0.25). Among them, reflectance at 655 nm showed the strongest correlation with J_a (r = 0.30).
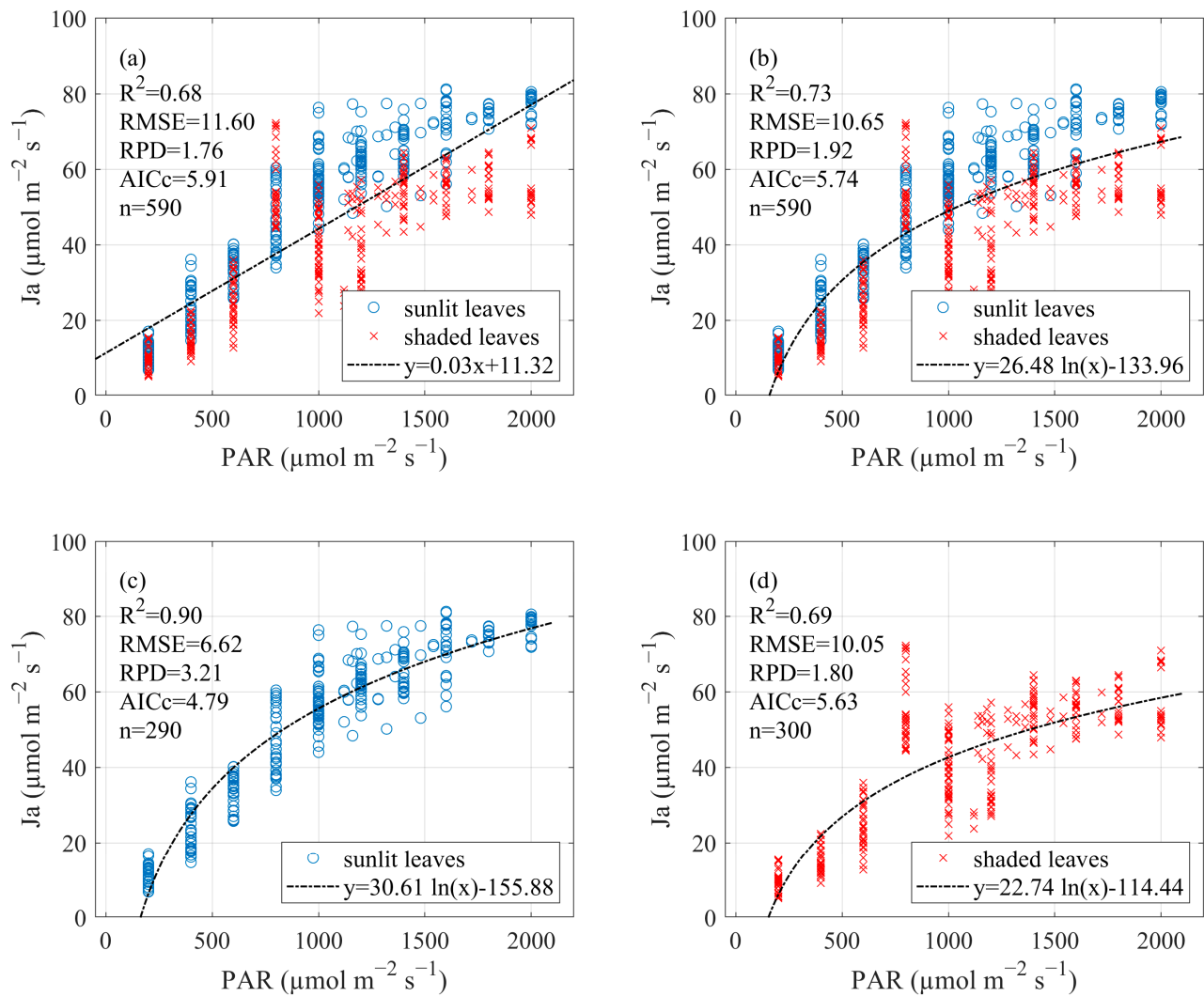
**Figure 2.** The relationship between the actual electron transport rate (J_a) and the incident light intensity: (**a**) polynomial regression for all leaves, (**b**) logarithmic regression for all leaves, (**c**) logarithmic regression for sunlit leaves, and (**d**) logarithmic regression for shaded leaves.

Figure 3. Relationship between actual electron transport rate and hyperspectral reflectance.

The model based on single-band reflectance at 655 nm was poor at estimating J_a, with an *RPD* value of 1.05 (Figure 4a). The SR index and the ND index using reflectance at 2070 nm and 2075 nm were the most effective in estimating J_a (R^2 = 0.25, *RPD* = 1.16, *RMSE* = 17.65, *AICc* = 6.75) (Figure 4b,d). The results show that the model using one- or two-band vegetation indices was not effective (poor) in estimating the actual electron transport rate.
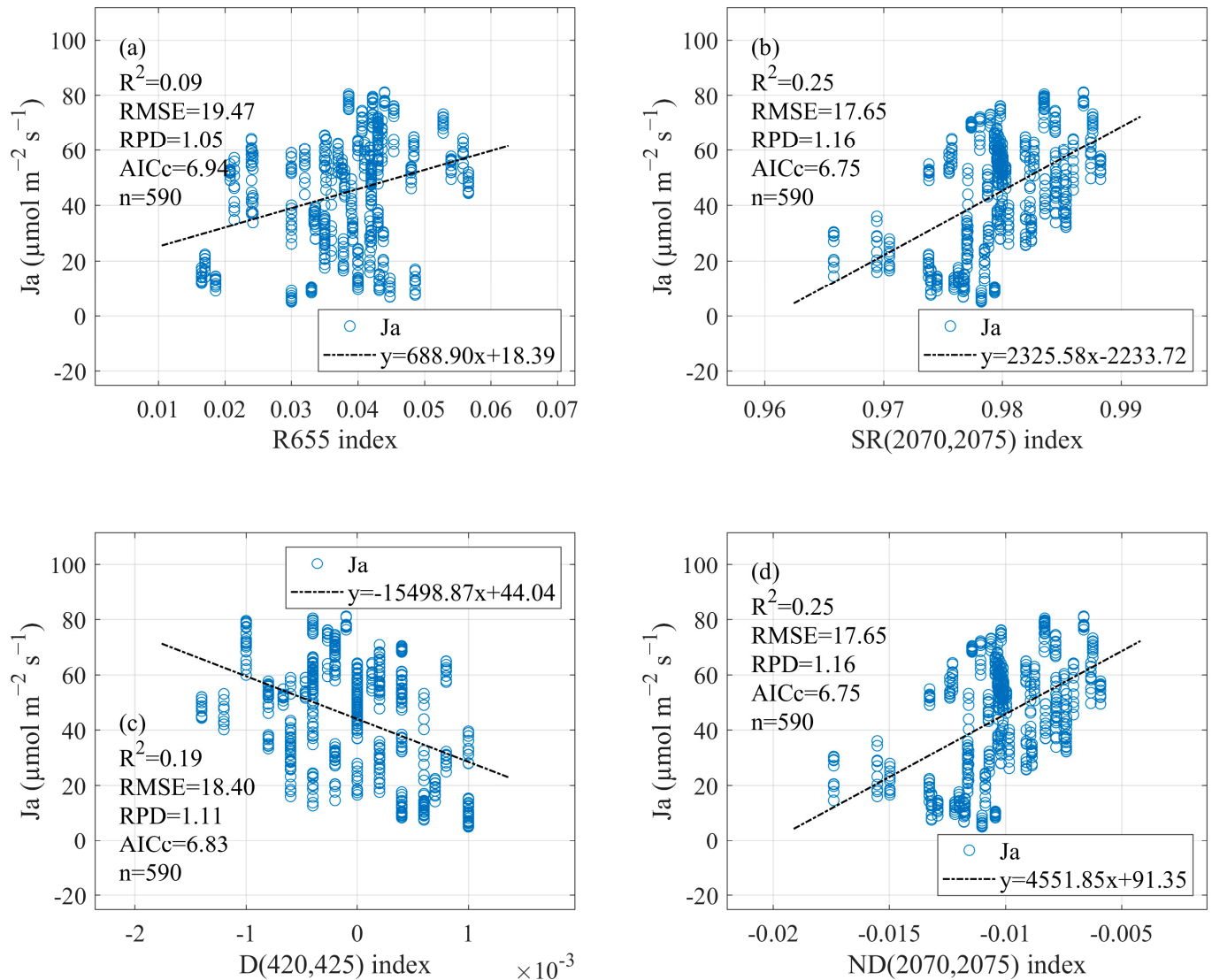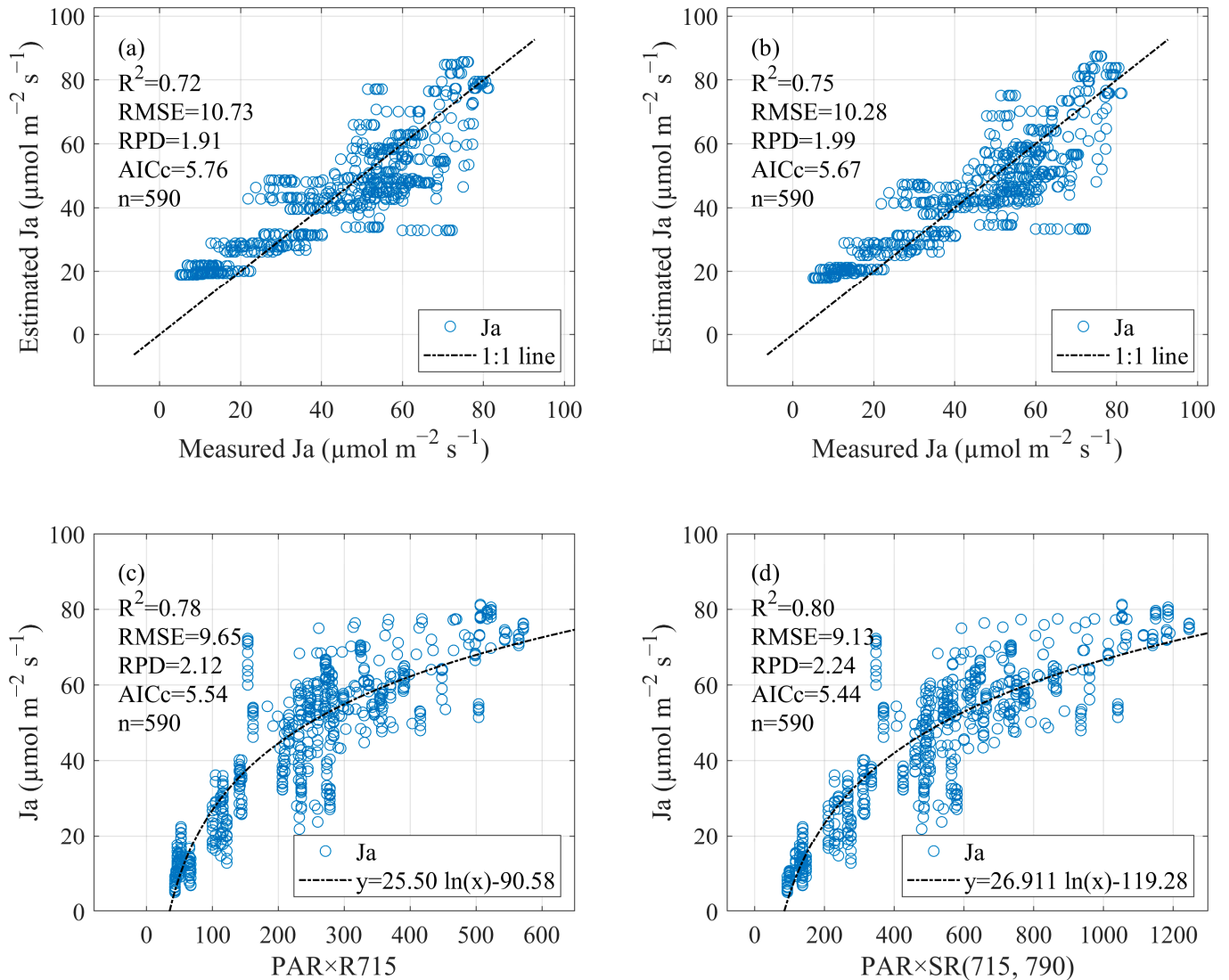

Figure 4. Scatter plots of the measured leaf actual electron transport rate (J_a) and model-estimated J_a values with spectral indices derived from leaf reflectance: (**a**) the single-band R655 index, (**b**) the two-band simple ratio index SR (2070, 2075), (**c**) the two-band difference index D (420, 425), and (**d**) the two-band normalized difference index ND (2070, 2075).

3.3. Estimation of Actual Electron Transport Rate with Both Incident Light Intensity and Reflectance

The actual electron transport rate was then estimated using Equation (5) with both incident light intensity and leaf reflectance. Among all single-band models, the coupling of reflectance values at 715 nm with incident light intensity showed the best performance in tracking the variation in the actual leaf electron transport rate (J_a) (Figure 5a). The relationship between the measured actual leaf electron transport rate and the estimated values with PAR and reflectance at 715 nm is shown in Figure 5a. The accuracy of this model can be classified as good, as the *RPD* value of this model was 1.91. The R^2 value between the measured and estimated values was 0.72, and the *RMSE* for the model prediction of

the actual leaf electron transport rate was 10.73 μmol m^{-2} s^{-1}. Additionally, combining the simple ratio index using reflectance values at 715 nm and 790 nm with incident light intensity demonstrated superior performance compared to single-band models (Figure 5b). The *RPD* value of this model was 1.99.

Figure 5. The relationship between the estimated and measured leaf actual electron transport rate (J_a) values. (**a**) A scatter plot of the measured J_a and estimated values coupling PAR and leaf reflectance at 715 nm fitted using the linear-to -first-order polynomial regression, (**b**) a scatter plot of the measured J_a and estimated values coupling PAR and the SR (715, 790) index fitted using the linear-to-first-order polynomial regression, (**c**) a scatter plot of the measured J_a and PAR times leaf reflectance at 715 nm fitted using logarithmic regression, and (**d**) a scatter plot of the measured J_a and PAR times the SR (715, 790) index fitted using logarithmic regression.

The logarithmic regression method proved to be more effective in estimating the actual electron transport rate from incident light intensity and leaf reflectance-based *VIs* (Figure 5c,d). The model constructed using polynomial regression demonstrated good predictive capabilities with regard to the coupling of PAR and leaf reflectivity. The *RPD* value of the model coupling PAR and single-band leaf reflectance at 715 nm was 2.12. In addition, the *RPD* value of the model coupling PAR and the two-band simple ratio index (SR) (715, 790) reached 2.24. The *AICc* value of this model coupling PAR and the SR (715, 790) index was 5.44, which was lower than the values of the models based on PAR

alone (5.74 shown in Figure 2b) or the spectral index alone (6.75 shown in Figure 4b,d). Both *RPD* and *AICc* values indicate that the model coupling PAR and the two-band simple ratio index (SR) (715, 790) was more effective in tracking the variation in the actual electron transport rate.

4. Discussion

4.1. Estimation of Actual Electron Transport Rate from Hyperspectral Reflectance and Vegetation Indices

Hyperspectral remote sensing has become a valuable method for estimating various physiological parameters in plants, including the electron transport rate [32,35,54,55]. This technology captures reflectance data over a wide range of narrow spectral bands, allowing for a detailed analysis of plant characteristics. Several studies have identified specific hyperspectral bands or indices that are sensitive to changes in photosynthetic activity, which is directly related to leaf electron transport rates [41].

The red edge refers to a narrow spectral band situated between the red and near-infrared (NIR) wavelengths, spanning 680–750 nm, where there is a sharp increase in reflectance due to chlorophyll absorption. This region is highly sensitive to changes in photosynthetic activity [56]. Our results show that reflectance at 715 nm combined with light intensity could accurately predict the actual electron transport rate in all leaves, which is consistent with previous studies.

Furthermore, near-infrared (NIR) reflectance has been proposed as an important band to quantify the status of electron transport chain dynamics [57]. The reflectance in the NIR band region is influenced by both the leaf water content and the internal leaf structure. These factors are related to the photosynthetic capacity and overall health of the leaf and indirectly affect the electron transport rate [58]. In addition, the bands around 760 nm are typically used for retrieving chlorophyll fluorescence [31]. These bands may be useful for estimating the electron transport rate, as a strong relationship between chlorophyll fluorescence and photosynthesis has been shown [59–63]. The correlation patterns between chlorophyll fluorescence parameters and reflectance are identifiable in the NIR band [64]. We also found that reflectance values within 760–1320 nm were effective in determining the actual electron transport rate in sunlit leaves.

4.2. Calculation of Actual Electron Transport Rate under Different Light Conditions

In the commonly used FvCB model, the actual electron transport rate has been estimated as a function of PAR, the leaf absorbance (α), J_{max}, and the curvature factor (θ) related to the transition between the light-limited photosynthesis phase and the light-saturated photosynthesis phase [6,65,66]. Among these parameters, the intensity of incident light or the amount of PAR is critical in determining the electron transport rate in leaves [67,68].

Our findings indicate that the actual electron transfer rate (J_a) of mango leaves exhibited a positive correlation with increasing light intensity. At PAR values below 1000 μmol m^{-2} s^{-1}, no significant difference was observed between the leaf groups exposed to sunlight and those in the shade. At PAR exceeding 1000 μmol m^{-2} s^{-1}, the electron transport rates (J_a) of sun-exposed leaves were found to be significantly higher than those of shaded leaves. Sunlit leaves are adapted to high light intensity, which significantly increases their photosynthetic capacity. Thus, sunlit leaves typically exhibit higher photosynthetic rates and are more efficient in using the available light [69,70]. In contrast, shaded leaves receive lower light intensities and have adapted to maximize their photosynthetic efficiency under these conditions. They typically have a lower electron transport rate than sunlit leaves due to the reduced availability of light energy [71]. However, shaded leaves compensate by having a higher chlorophyll b-to-chlorophyll a ratio, which allows them to capture the limited light more efficiently [72].

4.3. Inference of Actual Electron Transport Rate from Both Incident Light and Reflectance and Their Relative Importance

Hyperspectral reflectance can be used to infer biochemical or physiological properties of plants [31,32]. It has been demonstrated that photosynthetic capacity parameters can be retrieved from hyperspectral reflectance spectra [39,73]. Various spectral indices or multiple regression models have been proposed to estimate V_{cmax} and J_{max} (typically measured at a reference temperature such as 25 °C) from hyperspectral data [35,37,38,40].

However, real-time photosynthetic activities are influenced by both environmental conditions and plant biochemistry [66]. Calculation of the leaf-level electron transport rate in physiological models has always included leaf absorbance, the photosynthetic photon flux density absorbed by the leaf, and other parameters [74]. Therefore, to accurately model the real-time electron transport rate, both incident light and reflectance must be considered. Liran et al. (2020) proposed calculating the electron transport rate by using the product of PAR, the NDVI, and solar-induced fluorescence [41]. In this study, we also found that coupling incident light and reflectance improved the predictive performance for estimating the actual leaf electron transport rate (J_a). The accuracy of the model using both incident light and reflectance can be classified as having a very good prediction (RPD = 2.12 for single-band reflectance and RPD = 2.24 for the two-band SR index), while the model using incident light provided only a good (RPD = 1.92) prediction. The model using the reflectance-based spectral index gave a poor prediction (RPD = 1.16). The results obtained in this study prove that the integration of incident light data with hyperspectral reflectance measurements provides a robust approach to infer the real-time electron transport rate.

In the model coupling PAR and the single-band reflectance index, the relative importance [75] of PAR and the index R715 for the estimation of the actual electron transport rate was 93.59% and 6.41%, respectively, while in the model coupling PAR and the two-band index SR (715, 790), the relative importance of PAR and the index was 92.69% and 7.31%, respectively.

4.4. Differences between Leaves Exposed to Sunlight and Leaves in Shade

The developed model (see Figure 5c) in this study combining both leaf reflectance at 715 nm and incident light intensity could track the variation in the electron transport rate for all leaf samples. However, the physiological behavior of leaves can vary significantly depending on their exposure to sunlight [76–78]. Furthermore, the spectral characteristics of sunlit leaves and shaded leaves may exhibit notable discrepancies [71,79]. As a result, the correlation coefficients of leaf reflectance and the actual electron transport rate were quite different between the sunlit and shaded leaves, and the correlation between the actual leaf electron transport rate and the reflectance of shaded leaves was stronger compared to that of sunlit leaves (Figure 6). The results are in agreement with previous reports of hyperspectral remote sensing of physiological parameters, which include the maximum rate of photosynthetic electron transport [36], the maximum quantum yield for whole-chain electron transport [71], and chlorophyll fluorescence [47]. The combination of light intensity and leaf reflectance greatly improves the accuracy of predicting the actual leaf electron transport rate of sunlit leaves. The J_a of sunlit leaves can be predicted with an RPD value of around 2.60 (excellent performance) using light intensity and reflectance in a single band within 760–1320 nm. However, for shaded leaves, the actual electron transport rate can only be predicted with a lower RPD value of 1.73 (fair performance) using light intensity and reflectance at 685 nm.
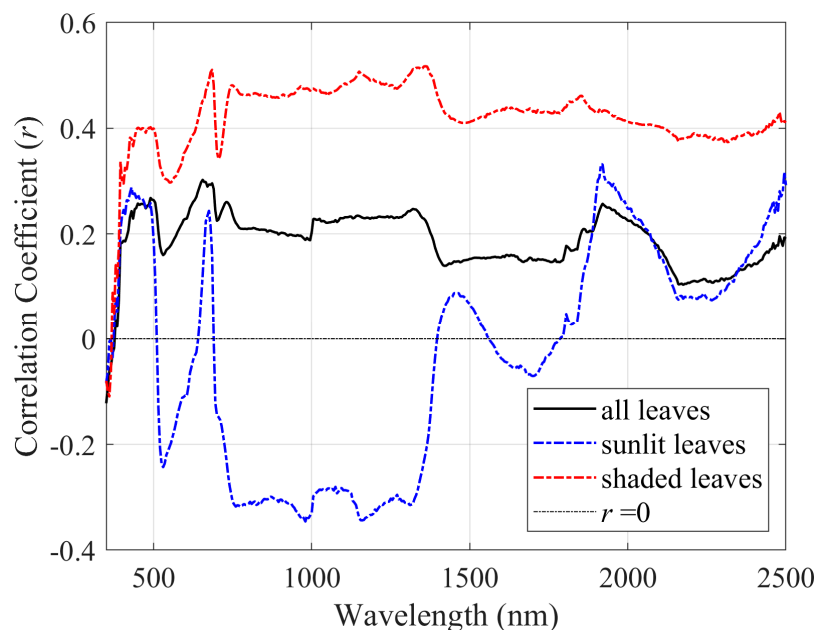
Figure 6. Correlation coefficients of leaf reflectance value and actual electron transport rate for sunlit and shaded leaves.

5. Conclusions

This study attempted to combine both incident light intensity and hyperspectral reflectance data for real-time quantification of the actual electron transport rate (J_a) in mango leaves. Our results have shown that the actual leaf electron transport rate can be accurately estimated using a combination of incident light intensity and leaf reflectance. A more accurate model was developed specifically for sunlit leaves, which can reach an *RPD* value of about 2.60 using light intensity and reflectance in a single band within 760–1320 nm. We anticipate that the practical approach of this study will enhance our understanding of the electron transport rate in real time, offering a method to monitor dynamic photosynthetic responses to climatic conditions.

References

1. Damm, A.; Guanter, L.; Paul-Limoges, E.; van der Tol, C.; Hueni, A.; Buchmann, N.; Eugster, W.; Ammann, C.; Schaepman, M.E. Far-red sun-induced chlorophyll fluorescence shows ecosystem-specific relationships to gross primary production: An assessment based on observational and modeling approaches. *Remote Sens. Environ.* **2015**, *166*, 91–105. [CrossRef]
2. Merrick, T.; Jorge, M.L.S.P.; Silva, T.S.F.; Pau, S.; Rausch, J.; Broadbent, E.N.; Bennartz, R. Characterization of chlorophyll fluorescence, absorbed photosynthetically active radiation, and reflectance-based vegetation index spectroradiometer measurements. *Int. J. Remote Sens.* **2020**, *41*, 6755–6782. [CrossRef]

3. Zhang, Y.; Guanter, L.; Berry, J.A.; van der Tol, C.; Yang, X.; Tang, J.; Zhang, F. Model-based analysis of the relationship between sun-induced chlorophyll fluorescence and gross primary production for remote sensing applications. *Remote Sens. Environ.* **2016**, *187*, 145–155. [CrossRef]

4. Zhang, Z.; Xiong, J.; Fan, M.; Tao, M.; Wang, Q.; Bai, Y. Satellite-observed vegetation responses to aerosols variability. *Agric. For. Meteorol.* **2023**, *329*, 109278. [CrossRef]

5. Chen, J.M.; Wang, R.; Liu, Y.; He, L.; Croft, H.; Luo, X.; Wang, H.; Smith, N.G.; Keenan, T.F.; Prentice, I.C.; et al. Global datasets of leaf photosynthetic capacity for ecological and earth system research. *Earth Syst. Sci. Data* **2022**, *14*, 4077–4093. [CrossRef]

6. Farquhar, G.D.; von Caemmerer, S.; Berry, J.A. A biochemical model of photosynthetic CO_2 assimilation in leaves of C_3 species. *Planta* **1980**, *149*, 78–90. [CrossRef]

7. Sharkey, T.D.; Bernacchi, C.J.; Farquhar, G.D.; Singsaas, E.L. Fitting photosynthetic carbon dioxide response curves for C_3 leaves. *Plant Cell Environ.* **2007**, *30*, 1035–1040. [CrossRef]

8. Buckley, T.N.; Farquhar, G.D. A new analytical model for whole-leaf potential electron transport rate. *Plant Cell Environ.* **2004**, *27*, 1487–1502. [CrossRef]

9. Han, J.; Chang, C.Y.Y.; Gu, L.; Zhang, Y.; Meeker, E.W.; Magney, T.S.; Walker, A.P.; Wen, J.; Kira, O.; McNaull, S.; et al. The physiological basis for estimating photosynthesis from Chla fluorescence. *New Phytol.* **2022**, *234*, 1206–1219. [CrossRef]

10. Wang, G.; Zeng, F.; Song, P.; Sun, B.; Wang, Q.; Wang, J. Effects of reduced chlorophyll content on photosystem functions and photosynthetic electron transport rate in rice leaves. *J. Plant Physiol.* **2022**, *272*, 153669. [CrossRef]

11. von Caemmerer, S.; Farquhar, G.D. Some relationships between the biochemistry of photosynthesis and the gas exchange of leaves. *Planta* **1981**, *153*, 376–387. [CrossRef] [PubMed]

12. Tsuyama, M.; Shibata, M.; Kobayashi, Y. Leaf factors affecting the relationship between chlorophyll fluorescence and the rate of photosynthetic electron transport as determined from CO_2 uptake. *J. Plant Physiol.* **2003**, *160*, 1131–1139. [CrossRef] [PubMed]

13. Gitelson, A.; Arkebauer, T.; Viña, A.; Skakun, S.; Inoue, Y. Evaluating plant photosynthetic traits via absorption coefficient in the photosynthetically active radiation region. *Remote Sens. Environ.* **2021**, *258*, 112401. [CrossRef]

14. Leong, T.-Y.; Anderson, J.M. Adaptation of the thylakoid membranes of pea chloroplasts to light intensities. II. Regulation of electron transport capacities, electron carriers, coupling factor (CF1) activity and rates of photosynthesis. *Photosynth. Res.* **1984**, *5*, 117–128. [CrossRef]

15. Moualeu-Ngangue, D.P.; Chen, T.-W.; Stützel, H. A new method to estimate photosynthetic parameters through net assimilation rate−intercellular space CO_2 concentration (A−Ci) curve and chlorophyll fluorescence measurements. *New Phytol.* **2017**, *213*, 1543–1554. [CrossRef]

16. Sharkey, T.D. What gas exchange data can tell us about photosynthesis. *Plant Cell Environ.* **2016**, *39*, 1161–1163. [CrossRef]

17. Bellasio, C.; Beerling, D.J.; Griffiths, H. An Excel tool for deriving key photosynthetic parameters from combined gas exchange and chlorophyll fluorescence: Theory and practice. *Plant Cell Environ.* **2016**, *39*, 1180–1197. [CrossRef]

18. Medlyn, B.E.; Dreyer, E.; Ellsworth, D.; Forstreuter, M.; Harley, P.C.; Kirschbaum, M.U.F.; Le Roux, X.; Montpied, P.; Strassemeyer, J.; Walcroft, A.; et al. Temperature response of parameters of a biochemically based model of photosynthesis. II. A review of experimental data. *Plant Cell Environ.* **2002**, *25*, 1167–1179. [CrossRef]

19. Kattge, J.; Knorr, W. Temperature acclimation in a biochemical model of photosynthesis: A reanalysis of data from 36 species. *Plant Cell Environ.* **2007**, *30*, 1176–1190. [CrossRef]

20. Medlyn, B.E.; Loustau, D.; Delzon, S. Temperature response of parameters of a biochemically based model of photosynthesis. I. Seasonal changes in mature maritime pine (*Pinus pinaster* Ait.). *Plant Cell Environ.* **2002**, *25*, 1155–1165. [CrossRef]

21. Gu, L.; Han, J.; Wood, J.D.; Chang, C.Y.-Y.; Sun, Y. Sun-induced Chl fluorescence and its importance for biophysical modeling of photosynthesis based on light reactions. *New Phytol.* **2019**, *223*, 1179–1191. [CrossRef] [PubMed]

22. Wang, Y.; Frankenberg, C. Toward More Accurate Modeling of Canopy Radiative Transfer and Leaf Electron Transport in Land Surface Modeling. *J. Adv. Model. Earth Syst.* **2024**, *16*, e2023MS003992. [CrossRef]

23. Liu, L.; Guan, L.; Liu, X. Directly estimating diurnal changes in GPP for C3 and C4 crops using far-red sun-induced chlorophyll fluorescence. *Agric. For. Meteorol.* **2017**, *232*, 1–9. [CrossRef]

24. Wu, Y.; Zhang, Z.; Zhang, X.; Wu, L.; Zhang, Y. How do sky conditions affect the relationships between ground-based solar-induced chlorophyll fluorescence and gross primary productivity across different plant types? *J. Geophys. Res.-Biogeosci.* **2022**, *127*, e2022JG006865. [CrossRef]

25. Kim, J.; Ryu, Y.; Dechant, B.; Lee, H.; Kim, H.S.; Kornfeld, A.; Berry, J.A. Solar-induced chlorophyll fluorescence is non-linearly related to canopy photosynthesis in a temperate evergreen needleleaf forest during the fall transition. *Remote Sens. Environ.* **2021**, *258*, 112362. [CrossRef]

26. Yang, K.; Ryu, Y.; Dechant, B.; Berry, J.A.; Hwang, Y.; Jiang, C.; Kang, M.; Kim, J.; Kimm, H.; Kornfeld, A.; et al. Sun-induced chlorophyll fluorescence is more strongly related to absorbed light than to photosynthesis at half-hourly resolution in a rice paddy. *Remote Sens. Environ.* **2018**, *216*, 658–673. [CrossRef]

27. Li, Z.; Zhang, Q.; Li, J.; Yang, X.; Wu, Y.; Zhang, Z.; Wang, S.; Wang, H.; Zhang, Y. Solar-induced chlorophyll fluorescence and its link to canopy photosynthesis in maize from continuous ground measurements. *Remote Sens. Environ.* **2020**, *236*, 111420. [CrossRef]

28. Yang, P.; van der Tol, C.; Campbell, P.K.E.; Middleton, E.M. Unraveling the physical and physiological basis for the solar—Induced chlorophyll fluorescence and photosynthesis relationship using continuous leaf and canopy measurements of a corn crop. *Biogeosciences* **2021**, *18*, 441–465. [CrossRef]

29. Mohammed, G.H.; Colombo, R.; Middleton, E.M.; Rascher, U.; van der Tol, C.; Nedbal, L.; Goulas, Y.; Pérez-Priego, O.; Damm, A.; Meroni, M.; et al. Remote sensing of solar-induced chlorophyll fluorescence (SIF) in vegetation: 50 years of progress. *Remote Sens. Environ.* **2019**, *231*, 111177. [CrossRef]

30. van der Tol, C.; Berry, J.A.; Campbell, P.K.E.; Rascher, U. Models of fluorescence and photosynthesis for interpreting measurements of solar-induced chlorophyll fluorescence. *J. Geophys. Res.-Biogeosci.* **2014**, *119*, 2312–2327. [CrossRef]

31. Wu, L.; Zhang, Y.; Zhang, Z.; Zhang, X.; Wu, Y.; Chen, J.M. Deriving photosystem-level red chlorophyll fluorescence emission by combining leaf chlorophyll content and canopy far-red solar-induced fluorescence: Possibilities and challenges. *Remote Sens. Environ.* **2024**, *304*, 114043. [CrossRef]

32. Zhang, Y.; Migliavacca, M.; Penuelas, J.; Ju, W. Advances in hyperspectral remote sensing of vegetation traits and functions. *Remote Sens. Environ.* **2021**, *252*, 112121. [CrossRef]

33. Verrelst, J.; Camps-Valls, G.; Muñoz-Marí, J.; Rivera, J.P.; Veroustraete, F.; Clevers, J.G.P.W.; Moreno, J. Optical remote sensing and the retrieval of terrestrial vegetation bio-geophysical properties—A review. *ISPRS-J. Photogramm. Remote Sens.* **2015**, *108*, 273–290. [CrossRef]

34. Gamon, J.A.; Somers, B.; Malenovský, Z.; Middleton, E.M.; Rascher, U.; Schaepman, M.E. Assessing Vegetation Function with Imaging Spectroscopy. *Surv. Geophys.* **2019**, *40*, 489–513. [CrossRef]

35. Kumagai, E.; Burroughs, C.H.; Pederson, T.L.; Montes, C.M.; Peng, B.; Kimm, H.; Guan, K.; Ainsworth, E.A.; Bernacchi, C.J. Predicting biochemical acclimation of leaf photosynthesis in soybean under in-field canopy warming using hyperspectral reflectance. *Plant Cell Environ.* **2022**, *45*, 80–94. [CrossRef]

36. Jin, J.; Arief Pratama, B.; Wang, Q. Tracing Leaf Photosynthetic Parameters Using Hyperspectral Indices in an Alpine Deciduous Forest. *Remote Sens.* **2020**, *12*, 1124. [CrossRef]

37. Fu, P.; Meacham-Hensold, K.; Guan, K.; Wu, J.; Bernacchi, C. Estimating photosynthetic traits from reflectance spectra: A synthesis of spectral indices, numerical inversion, and partial least square regression. *Plant Cell Environ.* **2020**, *43*, 1241–1258. [CrossRef]

38. Fu, P.; Meacham-Hensold, K.; Guan, K.; Bernacchi, C.J. Hyperspectral Leaf Reflectance as Proxy for Photosynthetic Capacities: An Ensemble Approach Based on Multiple Machine Learning Algorithms. *Front. Plant Sci.* **2019**, *10*, 730. [CrossRef]

39. Song, G.; Wang, Q.; Jin, J. Estimation of leaf photosynthetic capacity parameters using spectral indices developed from fractional-order derivatives. *Comput. Electron. Agric.* **2023**, *212*, 108068. [CrossRef]

40. Jin, J.; Wang, Q.; Song, G. Selecting informative bands for partial least squares regressions improves their goodness-of-fits to estimate leaf photosynthetic parameters from hyperspectral data. *Photosynth. Res.* **2022**, *151*, 71–82. [CrossRef]

41. Liran, O.; Shir, O.M.; Levy, S.; Grunfeld, A.; Shelly, Y. Novel Remote Sensing Index of Electron Transport Rate Predicts Primary Production and Crop Health in *L. sativa* and *Z. mays*. *Remote Sens.* **2020**, *12*, 1718. [CrossRef]

42. Chen, R.; Liu, L.; Liu, Z.; Liu, X.; Kim, J.; Kim, H.S.; Lee, H.; Wu, G.; Guo, C.; Gu, L. SIF-based GPP modeling for evergreen forests considering the seasonal variation in maximum photochemical efficiency. *Agric. For. Meteorol.* **2024**, *344*, 109814. [CrossRef]

43. Song, G.; Wang, Q.; Zhuang, J.; Jin, J. Dynamics of leaf chlorophyll fluorescence parameters can well be tracked by coupling VIS-NIR-SWIR hyperspectral reflectance and light drivers in partial least-squares regression. *Sci. Hortic.* **2024**, *325*, 112651. [CrossRef]

44. Song, G.; Wang, Q.; Zhuang, J.; Jin, J. Timely estimation of leaf chlorophyll fluorescence parameters under varying light regimes by coupling light drivers to leaf traits. *Physiol. Plant.* **2023**, *175*, e14048. [CrossRef]

45. Jin, J.; Huang, N.; Huang, Y.; Yan, Y.; Zhao, X.; Wu, M. Proximal Remote Sensing-Based Vegetation Indices for Monitoring Mango Tree Stem Sap Flux Density. *Remote Sens.* **2022**, *14*, 1483. [CrossRef]

46. Zhuang, J.; Wang, Q.; Jin, J. Improved modeling of leaf stomatal conductance by incorporating its highly dynamic responses to varying light conditions in Mango species (*Mangifera indica* L.). *Sci. Hortic.* **2024**, *328*, 112894. [CrossRef]

47. Zhuang, J.; Wang, Q.; Song, G.; Jin, J. Validating and Developing Hyperspectral Indices for Tracing Leaf Chlorophyll Fluorescence Parameters under Varying Light Conditions. *Remote Sens.* **2023**, *15*, 4890. [CrossRef]

48. Von Caemmerer, S. *Biochemical Models of Leaf Photosynthesis*; Csiro Publishing: Collingwood, VIC, Australia, 2000.

49. Katul, G.; Manzoni, S.; Palmroth, S.; Oren, R. A stomatal optimization theory to describe the effects of atmospheric CO_2 on leaf photosynthesis and transpiration. *Ann. Bot.* **2009**, *105*, 431–442. [CrossRef]

50. Le Maire, G.; François, C.; Soudani, K.; Berveiller, D.; Pontailler, J.-Y.; Bréda, N.; Genet, H.; Davi, H.; Dufrêne, E. Calibration and validation of hyperspectral indices for the estimation of broadleaved forest leaf chlorophyll content, leaf mass per area, leaf area index and leaf canopy biomass. *Remote Sens. Environ.* **2008**, *112*, 3846–3864. [CrossRef]

51. Xue, J.; Su, B. Significant Remote Sensing Vegetation Indices: A Review of Developments and Applications. *J. Sens.* **2017**, *2017*, 1353691. [CrossRef]

52. Hurvich, C.M.; Tsai, C.-L. Regression and Time Series Model Selection in Small Samples. *Biometrika* **1989**, *76*, 297–307. [CrossRef]

53. Hong, Y.; Chen, S.; Liu, Y.; Zhang, Y.; Yu, L.; Chen, Y.; Liu, Y.; Cheng, H.; Liu, Y. Combination of fractional order derivative and memory-based learning algorithm to improve the estimation accuracy of soil organic matter by visible and near-infrared spectroscopy. *Catena* **2019**, *174*, 104–116. [CrossRef]

54. Terentev, A.; Badenko, V.; Shaydayuk, E.; Emelyanov, D.; Eremenko, D.; Klabukov, D.; Fedotov, A.; Dolzhenko, V. Hyperspectral Remote Sensing for Early Detection of Wheat Leaf Rust Caused by *Puccinia triticina*. *Agriculture* **2023**, *13*, 1186. [CrossRef]

55. Zhi, X.; Massey-Reed, S.R.; Wu, A.; Potgieter, A.; Borrell, A.; Hunt, C.; Jordan, D.; Zhao, Y.; Chapman, S.; Hammer, G.; et al. Estimating Photosynthetic Attributes from High-Throughput Canopy Hyperspectral Sensing in Sorghum. *Plant Phenomics* **2022**, *2022*, 9768502. [CrossRef] [PubMed]

56. Zhang, C.; Preece, C.; Filella, I.; Farré-Armengol, G.; Peñuelas, J. Assessment of the Response of Photosynthetic Activity of Mediterranean Evergreen Oaks to Enhanced Drought Stress and Recovery by Using PRI and R690/R630. *Forests* **2017**, *8*, 386. [CrossRef]

57. Falcioni, R.; Moriwaki, T.; Antunes, W.C.; Nanni, M.R. Rapid Quantification Method for Yield, Calorimetric Energy and Chlorophyll a Fluorescence Parameters in Nicotiana tabacum L. Using Vis-NIR-SWIR Hyperspectroscopy. *Plants* **2022**, *11*, 2406. [CrossRef]

58. Serrano, L.; Ustin, S.L.; Roberts, D.A.; Gamon, J.A.; Peñuelas, J. Deriving Water Content of Chaparral Vegetation from AVIRIS Data. *Remote Sens. Environ.* **2000**, *74*, 570–581. [CrossRef]

59. Pierrat, Z.; Magney, T.; Parazoo, N.C.; Grossmann, K.; Bowling, D.R.; Seibt, U.; Johnson, B.; Helgason, W.; Barr, A.; Bortnik, J.; et al. Diurnal and seasonal dynamics of solar-induced chlorophyll fluorescence, vegetation indices, and gross primary productivity in the boreal forest. *J. Geophys. Res.-Biogeosci.* **2022**, *127*, e2021JG006588. [CrossRef]

60. Liu, Y.; Chen, J.M.; He, L.; Zhang, Z.; Wang, R.; Rogers, C.; Fan, W.; de Oliveira, G.; Xie, X. Non-linearity between gross primary productivity and far-red solar-induced chlorophyll fluorescence emitted from canopies of major biomes. *Remote Sens. Environ.* **2022**, *271*, 112896. [CrossRef]

61. Hao, D.; Asrar, G.R.; Zeng, Y.; Yang, X.; Li, X.; Xiao, J.; Guan, K.; Wen, J.; Xiao, Q.; Berry, J.A.; et al. Potential of hotspot solar-induced chlorophyll fluorescence for better tracking terrestrial photosynthesis. *Glob. Chang. Biol.* **2021**, *27*, 2144–2158. [CrossRef]

62. Wu, G.; Guan, K.; Jiang, C.; Peng, B.; Kimm, H.; Chen, M.; Yang, X.; Wang, S.; Suyker, A.E.; Bernacchi, C.J.; et al. Radiance-based NIRv as a proxy for GPP of corn and soybean. *Environ. Res. Lett.* **2020**, *15*, 034009. [CrossRef]

63. Wang, X.; Chen, J.M.; Ju, W. Photochemical reflectance index (PRI) can be used to improve the relationship between gross primary productivity (GPP) and sun-induced chlorophyll fluorescence (SIF). *Remote Sens. Environ.* **2020**, *246*, 111888. [CrossRef]

64. Falcioni, R.; Antunes, W.C.; Oliveira, R.B.d.; Chicati, M.L.; Demattê, J.A.M.; Nanni, M.R. Assessment of Combined Reflectance, Transmittance, and Absorbance Hyperspectral Sensors for Prediction of Chlorophyll a Fluorescence Parameters. *Remote Sens.* **2023**, *15*, 5067. [CrossRef]

65. Sharkey, T.D. Photosynthesis in intact leaves of C_3 plants: Physics, physiology and rate limitations. *Bot. Rev.* **1985**, *51*, 53–105. [CrossRef]

66. Yin, X.; Busch, F.A.; Struik, P.C.; Sharkey, T.D. Evolution of a biochemical model of steady-state photosynthesis. *Plant Cell Environ.* **2021**, *44*, 2811–2837. [CrossRef] [PubMed]

67. Wang, G.G.; Bauerle, W.L. Effects of light intensity on the growth and energy balance of photosystem II electron transport in Quercus alba seedlings. *Ann. For. Sci.* **2006**, *63*, 111–118. [CrossRef]

68. Li, Y.; Xin, G.; Liu, C.; Shi, Q.; Yang, F.; Wei, M. Effects of red and blue light on leaf anatomy, CO_2 assimilation and the photosynthetic electron transport capacity of sweet pepper (*Capsicum annuum* L.) seedlings. *BMC Plant Biol.* **2020**, *20*, 318. [CrossRef]

69. Niinemets, Ü. Photosynthesis and resource distribution through plant canopies. *Plant Cell Environ.* **2007**, *30*, 1052–1071. [CrossRef]

70. Pearcy, R.W.; Muraoka, H.; Valladares, F. Crown architecture in sun and shade environments: Assessing function and trade-offs with a three-dimensional simulation model. *New Phytol.* **2005**, *166*, 791–800. [CrossRef]

71. Stratoulias, D.; Tóth, V.R. Photophysiology and Spectroscopy of Sun and Shade Leaves of *Phragmites australis* and the Effect on Patches of Different Densities. *Remote Sens.* **2020**, *12*, 200. [CrossRef]

72. Lichtenthaler, H.K.; Buschmann, C.; Döll, M.; Fietz, H.J.; Bach, T.; Kozel, U.; Meier, D.; Rahmsdorf, U. Photosynthetic activity, chloroplast ultrastructure, and leaf characteristics of high-light and low-light plants and of sun and shade leaves. *Photosynth. Res.* **1981**, *2*, 115–141. [CrossRef] [PubMed]

73. Zhou, Y.-A.; Zhai, L.; Zhou, W.; Zhou, J.; Cen, H. Investigation on data fusion of sun-induced chlorophyll fluorescence and reflectance for photosynthetic capacity of rice. *arXiv* **2023**, arXiv:2312.00437.

74. Hikosaka, K.; Noda, H.M. Modeling leaf CO_2 assimilation and Photosystem II photochemistry from chlorophyll fluorescence and the photochemical reflectance index. *Plant Cell Environ.* **2019**, *42*, 730–739. [CrossRef] [PubMed]

75. Groemping, U. Relative Importance for Linear Regression in R: The Package relaimpo. *J. Stat. Softw.* **2006**, *17*, 1–27. [CrossRef]

76. Song, G.; Wang, Q.; Jin, J. Leaf Photosynthetic Capacity of Sunlit and Shaded Mature Leaves in a Deciduous Forest. *Forests* **2020**, *11*, 318. [CrossRef]

77. Zhen, S.; van Iersel, M.W.; Bugbee, B. Photosynthesis in sun and shade: The surprising importance of far-red photons. *New Phytol.* **2022**, *236*, 538–546. [CrossRef]

78. Zhang, Z.; Chen, J.M.; Zhang, Y.; Li, M. Improving the ability of solar-induced chlorophyll fluorescence to track gross primary production through differentiating sunlit and shaded leaves. *Agric. For. Meteorol.* **2023**, *341*, 109658. [CrossRef]
79. Yu, Q.; Mickler, R.A.; Liang, T.; Liu, Y.; Jiang, J.; Song, K.; Wang, S. Hyperspectral differences between sunlit and shaded leaves in a Manchurian ash canopy in Northeast China. *Remote Sens. Lett.* **2022**, *13*, 800–811. [CrossRef]